Journal of Rock Mechanics and Geotechnical Engineering 10 (2018) 624–634

Contents lists available at ScienceDirect

Journal of Rock Mechanics and Geotechnical Engineering

journal homepage: www.rockgeotech.org

Full Length Article

Responses of jointed rock masses subjected to impact loading

Shabnam Aziznejad [a], Kamran Esmaieli [a,*], John Hadjigeorgiou [a], Denis Labrie [b]

[a] Lassonde Institute of Mining, University of Toronto, Toronto, Ontario M5S 3E3, Canada
[b] CanmetMINING, Natural Resources Canada, Ottawa, Ontario K1A 0G1, Canada

ARTICLE INFO

Article history:
Received 18 September 2017
Received in revised form
6 December 2017
Accepted 9 December 2017
Available online 7 April 2018

Keywords:
Jointed rock mass
Impact loading
Microcracks
Rock damage

ABSTRACT

Impact-induced damage to jointed rock masses has important consequences in various mining and civil engineering applications. This paper reports a numerical investigation to address the responses of jointed rock masses subjected to impact loading. It also focuses on the static and dynamic properties of an intact rock derived from a series of laboratory tests on meta-sandstone samples from a quarry in Nova Scotia, Canada. A distinct element code (PFC2D) was used to generate a bonded particle model (BPM) to simulate both the static and dynamic properties of the intact rock. The calibrated BPM was then used to construct large-scale jointed rock mass samples by incorporating discrete joint networks of multiple joint intensities into the intact rock matrix represented by the BPM. Finally, the impact-induced damage inflicted by a rigid projectile particle on the jointed rock mass samples was determined through the use of the numerical model. The simulation results show that joints play an important role in the impact-induced rock mass damage where higher joint intensity results in more damage to the rock mass. This is mainly attributed to variations of stress wave propagation in jointed rock masses as compared to intact rock devoid of joints.

1. Introduction

In many civil and mining engineering applications, rock materials are subjected to dynamic loading. They often have to withstand not only static loads but also impact loads due to explosions or collisions with other objects (e.g. drill bits, other rock boulders). Drill-and-blast method is commonly used for rock fragmentation in mining and civil engineering. During percussive drilling, the drilling bit continuously hits the rock materials in order to break the rock and make a hole. In blasting, a rock mass is subjected to a dynamic shock generated by explosives. Another example of impact loading can be found in ore pass systems, in underground mines, that are commonly used to transfer ore or waste from one mining level to a lower level using gravity. Collision of broken materials, flowing in an ore pass, with the ore pass walls can cause impact-induced damage and result in wear along the ore pass (Goodwill et al., 1999; Esmaieli and Hadjigeorgiou, 2011, 2014). In all of these examples, the rock fracture mechanism and fragmentation process occur under impact loading conditions. Hence, the behavior of rock under impact loading is of interest and importance.

Modeling the responses of rock materials under dynamic impact load is difficult given the transient nature of loading. According to Hiermaier (2013), under impact loading conditions, two basic processes occur: a change in the mechanical behavior of the material as a function of the strain rate, and the evolution and propagation of shock waves. Although many studies on rock material response under static conditions can be found in the literature, fewer studies have been reported on the behaviors of rocks under dynamic loading due to their higher complexity. In addition, the presence of pre-existing discontinuities in rocks such as joints, bedding planes, and foliations can significantly influence the responses of rock materials under both static and dynamic loads.

There are several laboratory experimental methods to quantify the responses of rock materials to impact loading (Camacho and Ortiz, 1996; Xia and Ahrens, 2001; Momber, 2003; Grange et al., 2008; Gao et al., 2010; Cao et al., 2011; Hiermaier, 2013). There are theoretical models for the evolution of rock damage under impact loading (Taylor et al., 1986; Ahrens and Rubin, 1993; Cao et al., 2011). Although dynamic impact laboratory testing of small intact rock samples is straightforward, impact testing of large rock mass samples is costly and inherently complex. An issue in these analytical models is that quite often there are too many parameters

* Corresponding author.
E-mail address: kamran.esmaeili@utoronto.ca (K. Esmaieli).
Peer review under responsibility of Institute of Rock and Soil Mechanics, Chinese Academy of Sciences.

https://doi.org/10.1016/j.jrmge.2017.12.006

involved and thus it is difficult to quantify them. Furthermore, only a few of the results of the analytical investigations can be confidently extrapolated to practical applications.

In the past, both continuum and discontinuum numerical modeling tools have been used to determine the behaviors of rocks under dynamic impact loading (Beus et al., 1999; Nazeri et al., 2002; Hu and Li, 2006; Grange et al., 2008; Wang and Tonon, 2010; Cao et al., 2011). Continuum-based numerical models are used to simulate rock damage by idealizing the material as a continuum and utilizing the degradation measurements in constitutive relations. Gao et al. (2010) simulated the dynamic impact loading of an intact rock using LS-DYNA, a finite element code, and analyzed the dynamic responses of the rock under impact loading. The simulation results were in agreement with the experimental ones and the model can then be used to describe the behaviors of the rock. Yilmaz and Unlu (2013) used a three-dimensional (3D) finite difference model, FLAC3D, to investigate the behaviors of two different rock masses subjected to blasting loads. They used empirical relationships to estimate the dynamic properties of each rock mass from its static properties. The Mohr-Coulomb failure criterion was then used to assess the blast-induced damage of the rock masses. In this study, the effect of rock mass jointing was implicitly considered through the constitutive model. Gong et al. (2006) used a two-dimensional (2D) distinct element model to investigate the effect of joint spacing on the penetration performance of a tunnel boring machine. They simulated a foliated rock mass and applied a constant normal force to the rock. Their results demonstrated that joint spacing had a strong influence on the resulting rock fragmentation, particularly where the growth of radial cracks was terminated at the joint interface. It can be argued that the normal force applied in this study was a quasi-static loading condition rather than a dynamic loading. More recently, Fakhimi and Lanari (2014) used a 2D bonded particle model (BPM) to simulate blast-induced rock damage around a 2D circular hole. They showed the effect of presence of a joint in the vicinity of the blast hole which reduced the transmitted shock wave and therefore decreased the number of cracks initiating and propagating beyond the joint surface. Furthermore, reflecting waves from the joint surface caused additional damage to the rock specimen around the hole. In the majority of these numerical modeling studies, only the static mechanical properties of rock were simulated and the models were not compared or calibrated against dynamic laboratory tests.

Despite several studies conducted on rock materials, a limited number of investigations have been carried out to quantify the impact-induced damage to jointed rock masses. This is significant as it is recognized that the geometrical distribution of pre-existing joints can influence the rock mass damage subjected to impact loading.

This paper aims to contribute to our understanding of impact-induced damage to jointed rock masses. It presents the results of a series of numerical simulations used to investigate the influence of joint intensity on the response of a jointed rock mass to impact loading. The numerical models were generated using the distinct element method. In this work, both the static and dynamic properties of an intact rock were simulated. Subsequently, jointed rock mass samples of various joint intensities were constructed in the models. These samples were subjected to impact loading and the inflicted damage on each rock mass sample was quantified.

2. Methodology

The static and dynamic properties of meta-sandstone intact rock samples, retrieved from a quarry in Nova Scotia, Canada, were determined in the laboratory. A distinct element code (PFC2D) was used to generate a BPM to simulate both the static and dynamic properties of intact rock. The calibrated intact rock model was subsequently used to develop large-scale jointed rock mass models by incorporating joint networks of different joint intensities into the BPM. Finally, the impact-induced damage inflicted by a rigid projectile particle on the jointed rock mass samples was determined.

2.1. Laboratory tests

The meta-sandstone samples obtained from a quarry were collected and tested at the CanmetMINING Rock Mechanics Laboratory, Natural Resources Canada (Ottawa, Ontario, Canada). The mineral composition of the rock was determined from polished sections through a scanning electron microscopy (SEM) analysis. The collected samples were comprised mainly of quartz and albite, with minor amounts of clinochlore, muscovite and calcite. The SEM examination of the samples showed 0.2–0.4 mm sub-rounded quartz grains with smaller 0.1–0.2 mm albite grains supported in a matrix composed of mostly clinochlore and some muscovite. No foliation or any other structures was observed in the rock samples.

The collected rock samples were subjected to a series of static and dynamic tests, including static uniaxial compression, static Brazilian, and dynamic drop tests. The static mechanical properties (uniaxial compressive strength (UCS), elastic modulus, Poisson's ratio, and indirect tensile strength) and dynamic properties (dynamic tensile strength) of the intact rock were determined at the CanmetMINING Rock Mechanics Laboratory.

2.1.1. Uniaxial compression tests

For the uniaxial compression tests, rock samples were prepared and tested according to ASTM D4543-08 (2008) and ASTM D7012-14 (2014), respectively. Uniaxial compression tests were carried out on samples with dimensions of 12 cm in height and 5 cm in diameter, using an MTS 815 load frame for quasi-static tests. During these tests, the axial load and deformation of samples were recorded. The elastic properties (Young's modulus and Poisson's ratio) were calculated from the linear portion of the stress–strain curve, over the range of 30%–70% of the sample ultimate compressive strength. Overall, 18 samples were tested for their UCSs.

2.1.2. Brazilian tests

The Brazilian test is commonly used as an indirect method for determining the tensile strength of intact rock in the laboratory. For static Brazilian tests, meta-sandstone samples were prepared in accordance with ASTM D3967-08 (2008). Tests were carried out using the MTS 815 load frame on samples with dimensions of 5 cm in diameter and 3 cm in thickness. Overall, 21 samples were tested using the Brazilian test procedure.

2.1.3. Drop tests

To determine the dynamic tensile strength of rock samples, dynamic drop tests were carried out using a vertical impact load frame Dynatup Model 9210 to replicate the conditions observed during impact loading of rock (Fig. 1). Tests were carried out with an impact mass of 19.35 kg, a drop height of 46 cm, with a total potential energy of 87 J in the system, and an impact velocity of 3 m/s. Impact tests were carried out on 44 core rock samples with diameter of 5 cm and thickness of 3 cm. The dynamic tensile strength of rock samples is higher than the static tensile strength of rock. The deflection in the drop test is the total displacement of a sample at the maximum dynamic load before it fails. This was measured by both strain gages and high-speed camera.

Table 1 summarizes the physico-mechanical properties of the intact rock measured in the laboratory. For each type of test, the number of samples, and the mean and standard deviation (S.D.) of the recorded mechanical properties are provided.

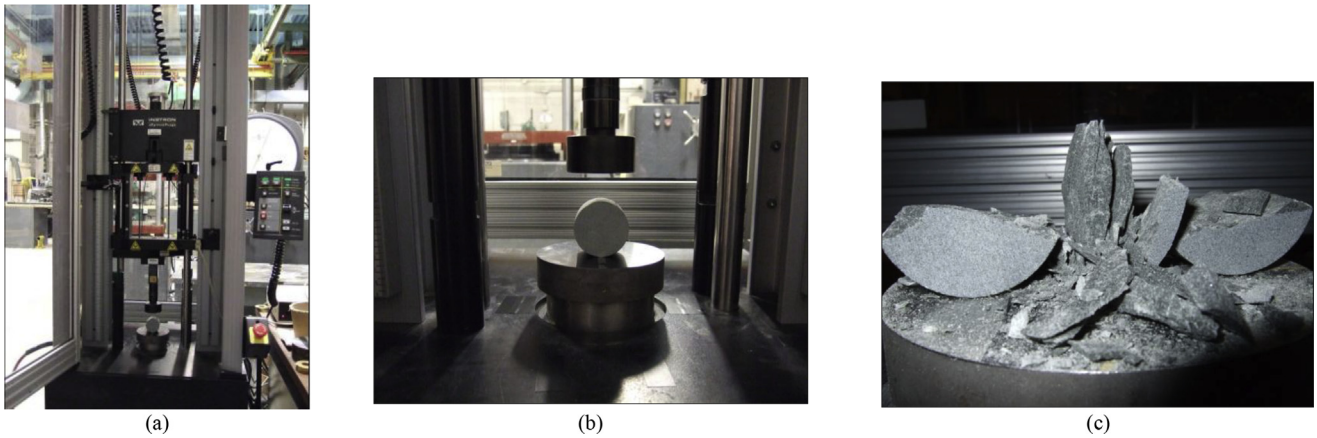

Fig. 1. (a) Dynatup 9210 load frame for dynamic impact tests, (b) Sample set-up ready for dynamic testing, and (c) Failed sample after dynamic test.

Table 1
Laboratory test results for meta-sandstone samples.

Type of test	Number of samples	Elastic modulus (GPa)		Poisson's ratio		Axial strain at peak (%)		UCS (MPa)		Static tensile strength (MPa)		Dynamic tensile strength (MPa)		Time to maximum load (ms)		Deflection (mm)	
		Mean	S.D.	Mean	S.D.	Mean	S.D.	Mean	S.D.	Mean	S.D.	Mean	S.D.	Mean	S.D.	Mean	S.D.
Uniaxial compression test	18	74.5	5	0.26	0.1	0.397	0.11	267	64								
Static Brazilian test	21									21.5	3						
Drop test	44											29.8	5	0.168	0.03	0.491	0.09

2.2. Numerical modeling

The objective of the numerical modeling was to replicate the results of the laboratory tests. This was a prelude to subsequent numerical experiments aiming to investigate the influence of scale and structure.

2.2.1. Simulation of the intact rock using BPM

The intact rock was simulated by a BPM using Itasca's PFC2D (Itasca, 2016). The BPM consists of a dense packing of non-uniform-sized circular rigid particles that are bonded together at their contact points. The procedure to generate a BPM has been presented by Potyondy and Cundall (2004). Newton's laws of motion relate corresponding particle motion to force and moment at each contact, which possesses finite normal and shear stiffnesses. Unlike the continuum numerical models, the BPM does not make the theoretical assumptions and suffers from the limitations on the constitutive material behavior. When a BPM is loaded, depending on the imposed levels of stress and strain, microcracks can initiate and develop within the model. Cracking is explicitly simulated as a bond breakage between the rigid particles. Microcracks are able to form, interact, and coalesce into macroscopic joints according to local conditions.

The first step in the material genesis procedure was the creation of a material vessel of equal dimensions as the laboratory test samples (12 cm high and 5 cm wide). The balls were randomly generated in the material vessel and the rock density values were applied to all the balls. The system was subsequently solved to achieve equilibrium and a dense packing of the circular particles. This was followed by bonding all contacts between circular particles using the flat-joint contact model.

Modeling the failure of hard brittle rock using the BPM has been improved over the past decade (Potyondy and Cundall, 2004; Cho et al., 2007; Potyondy, 2010, 2012, 2015). More recently, Potyondy (2015) summarized the major advancements in the BPM. Since its first introduction by Potyondy and Cundall (2004), the BPM has experienced significant improvements including clustered particle model (Potyondy and Cundall, 2004), clumped particle model (Cho et al., 2007), grain-based model (Potyondy, 2010), and finally flat-joint contact model (Potyondy, 2012). The improvements have mainly focused on reproducing the key characteristics of hard brittle rocks, namely, the high compressive to tensile strength ratio. The initial BPM developed by Potyondy and Cundall (2004) consists of parallel-bonded contact and suffers from the limitation of matching large ratios of UCS to tensile strength. In the parallel-bonded model, when the bond breaks, the interface between two circular disks no longer resists relative rotation and is fully debonded. The recently developed flat-joint contact model seems to have addressed this issue. In the flat-joint contact model, each contact simulates the behavior of an interface between two particles with locally flat notional surfaces, as shown in Fig. 2 (Potyondy, 2012). The interface is segmented, with each segment initially

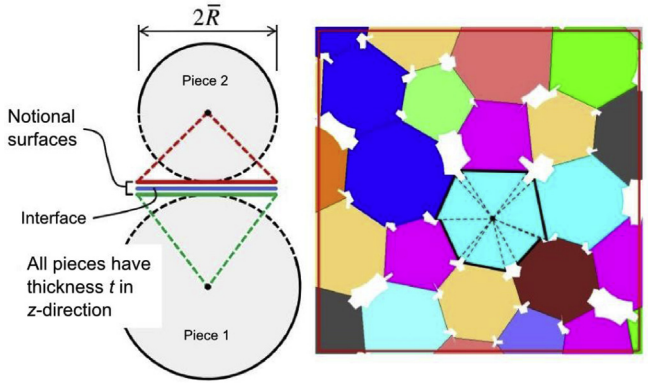

Fig. 2. 2D flat-joint contact (left) and flat-jointed material with effective surface of one grain highlighted (right) (Potyondy, 2012).

being bonded. A contact gap, a distance between the finite-size notional surfaces, is considered in the flat-joint contact model and presented in Fig. 2. As the bonded segments break, the interface behavior evolves from a fully bonded state to a fully debonded and frictional state. Since the flat-joint is not removed, even a fully broken interface continues to resist relative rotation. The continued moment-resisting ability is an important micro-structural feature of this model that makes it possible to match the representative ratio of the UCS to the tensile strength of the rock (Potyondy, 2012).

Fig. 3a shows the BPM generated to simulate the intact rock samples using flat-joint contact model. The dimensions are 12 cm × 5 cm (height × length). Fig. 3b shows a close-up view of the rigid circular balls bonded with flat-joint contacts. The flat-joint contacts in the model vary between 4 and 6 contacts.

2.2.2. Model calibration with static and dynamic properties of intact rock

The laboratory results were used to calibrate a BPM that simulates both static and dynamic properties of the intact rock. A BPM is characterized by its particle density, size distribution, as well as by the assembly and micro-properties of particles and contacts used in the model. The inverse calibration method was used to establish the necessary micro-properties, strength, and stiffness parameters for balls and contacts that simulate the laboratory intact rock material. To minimize the number of iterations, a systematic calibration procedure was undertaken, starting with reproducing the elastic constants of the rock. For simulation of a uniaxial compression test, the bond strength was set to a large value to prevent bond failure and to force the material to behave elastically. The Young's modulus was matched to the laboratory values by adjusting the elastic modulus for the flat-joint contacts. Subsequently, the Poisson's ratio was matched by varying the ratio of the contact normal to shear stiffness. A few iterations were necessary to match both values. Once the desired elastic response was obtained, the flat-joint contact tensile strength and cohesion were modified to match the UCS and tensile strength of the rock.

In the PFC2D model, the elastic constants (e.g. the Young's modulus and the Poisson's ratio) and the UCS are independent of particle size (Potyondy and Cundall, 2004). However, the Brazilian tensile strength exhibits a clear dependence on the particle size. The tensile strength decreases as the particle size is reduced. In this context, the particle size cannot be chosen arbitrarily (Potyondy and Cundall, 2004). For the calibration process, a minimum particle size of 0.3 mm was chosen, which is close to the minimum grain size of the rock samples.

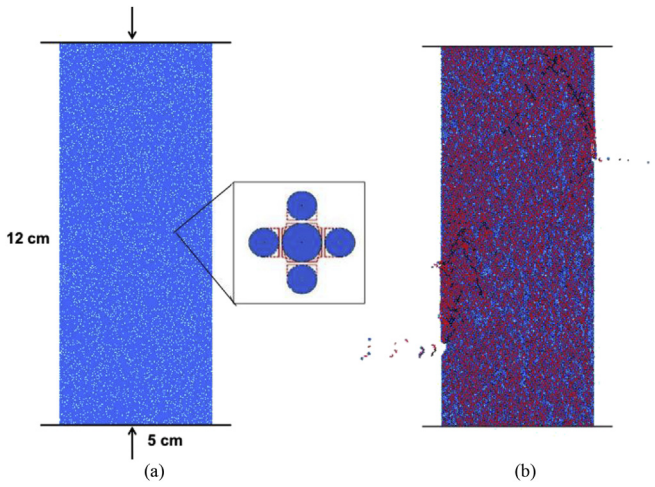

Fig. 3. (a) Simulation of the intact rock sample using BPM in PFC2D and effective interface geometry of flat-joint contact model between balls, and (b) Microcrack distribution within the sample after uniaxial compression test.

The uniaxial compression test was simulated by moving the top and bottom boundaries in order to load the BPM. During the test, the vertical forces acting on the boundaries and their displacement were recorded. This allowed measuring the axial stress and strain. Elastic properties (Young's modulus and Poisson's ratio) were calculated for the linear portion of the stress–strain curve at 50% of ultimate sample strength. Fig. 3b shows the initiation and propagation of microcracks during the compression test, which is presented in red color.

To simulate the Brazilian indirect tensile test, the sample was trimmed into a disk shape in contact with the model boundaries. Afterwards, the sample was loaded by moving the boundaries toward one another. During the test, the average force acting on the boundaries was monitored, and the maximum value was recorded to calculate the Brazilian tensile strength of the rock. Fig. 4 displays the microcracks, in red, developed within the BPM sample at the end of the Brazilian test. The macroscopic failure mode is tensile splitting, as illustrated in Fig. 4. This includes a major tensile fracture, parallel to the loading direction at the center of the sample, as well as some branching of fractures close to the diametrical axis.

To simulate an impact drop test with PFC2D, the sample was trimmed into a disk shape in contact with a frictionless bottom rigid boundary. The upper drop plate was simulated using the clump logic which allows the creation of a group of glued particles that behave as a single rigid body. Using the clump logic for plate simulation allowed assigning a particular weight to the plate and enabled a smooth contact between the drop plate and the rock sample. The properties of the drop plate clump are mass of 19.35 kg, impact velocity of clump 3 m/s, normal to shear stiffness ratio of 1, and friction coefficient of 0.5. The sample was loaded by dropping the plate on the sample. During the test, the impact force acting on the sample was recorded, and the maximum value was used to calculate the dynamic tensile strength of rock.

For calibration purposes, the properties of the contact between the drop plate and the test sample were established so as to achieve the same laboratory impact force on the sample. To better simulate a BPM subjected to a dynamic impact loading, it was necessary to set the local damping coefficient to a very low value and implement viscous damping to obtain realistic energy dissipation results (Itasca, 2016). Therefore, a low local damping of 0.1 was assigned to the particles in the sample. A linear contact model was assigned between the hitting clump and the model particles to satisfy the viscous damping conditions. Sensitivity analysis showed that increasing of normal damping ratio will slightly increase the amount of dissipated impact energy in the rock sample. As the drop test was normal to the sample, changing the shear damping ratio had no effect on the dissipated impact energy. Thus, the same value as the normal damping ratio was assigned to the shear damping ratio. The micro-properties used to calibrate the contact between the drop plate and the sample are the normal to shear damping ratio of 1, normal to shear stiffness ratio of 1, and elastic modulus of 60 GPa. The results of the initiation and propagation of microcracks during the drop test are shown in Fig. 5.

Under quasi static loading conditions, fracturing develops along a path requiring the least energy. Therefore, limited extension of microcracks can be found in the high strength areas due to the low overall stress and relaxation (Fig. 4). However, under impact loading conditions, cracks also develop along higher resistance areas because of the large amount of energy dissipation in very

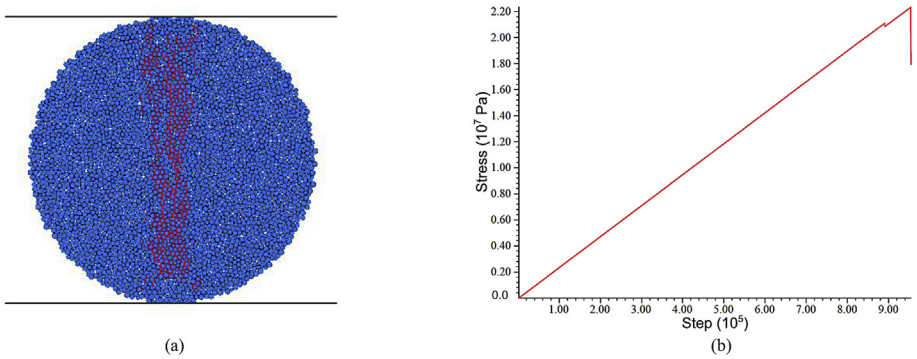

Fig. 4. (a) Microcrack distribution within the BPM for the simulated static Brazilian test, and (b) Plot of the Brazilian tensile stress test.

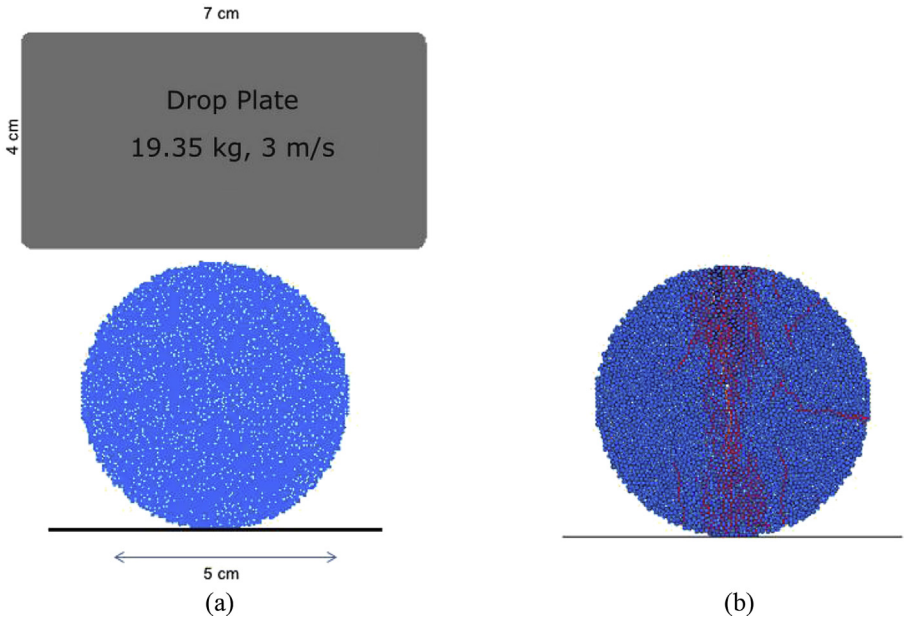

Fig. 5. (a) Simulated drop weight test, and (b) Microcracks developed within the BPM after the drop test.

short period of time (Fig. 5). Since relaxation cannot occur during this very short time, extensive microcracking develops due to the rapid increase of tensile stress (Cadoni, 2013).

Table 2 summarizes the micro-properties of the constructed BPM following the calibration process. The calibrated model shows a good agreement between the experimental and numerical results, with error levels being less than 10% (see Table 3). Moreover, the modes of failure observed in the laboratory tests are consistent with those simulated in the numerical models.

2.2.3. Simulation of a jointed rock mass

Laboratory testing of large rock samples under impact load poses significant experimental challenges. The results from large-scale samples have to be interpreted by recognizing the potential for material inhomogeneity. Following the laboratory tests on small samples, this work investigated the use of numerical models to potentially extrapolate the dynamic impact loading on large-scale jointed rock masses.

Once the intact rock model was calibrated for both static and dynamic properties, it was used to develop large-scale jointed rock mass samples by incorporating discrete joint networks into the BPM. This allowed for the generation of 2D synthetic rock mass (SRM) samples in which the BPM represents the rock material properties and a smooth-joint contact model (SJM) represents the joint network (Mas Ivars et al., 2008; Lambert and Coll, 2014). The mechanical behavior of a SRM sample depends on the combined behaviors of both the solid rock matrix and the embedded joint network (Esmaieli et al., 2015).

Table 2
Micro-mechanical properties of the calibrated BPM for both static and dynamic tests.

Element	Density (kg/m^3)	Minimum radius (mm)	Maximum to minimum radius ratio	Local damping factor	Contact gap (m)	Elastic modulus (GPa)	Normal to shear stiffness ratio	Friction angle (°)	Tensile strength (MPa)		Cohesion (MPa)	
									Mean	S.D.	Mean	S.D.
Ball Contact	2713	0.3	1.66	0.1	5×10^{-5}	65	3.3	0	35	25	120	50

Table 3
Comparison between experimental test results and the BPM simulation.

Uniaxial compression test												
Elastic modulus E			Poisson's ratio			Axial strain (%)			UCS		
Experimental (GPa)	PFC2D (GPa)	Error (%)	Experimental	PFC2D	Error (%)	Experimental	PFC2D	Error	Experimental (MPa)	PFC2D (MPa)	Error (%)
74.5	74.9	0.5	0.26	0.24	7.7	0.397	0.404	1.8	267	270	1.1
Static Brazilian test											
Static tensile strength			UCS/Tensile strength								
Experimental (MPa)	PFC2D (MPa)	Error (%)	Experimental	PFC2D	Error (%)						
21.4	22.3	4.2	12.5	12.1	3.2						
Drop test											
Maximum load			Dynamic tensile strength								
Experimental (kN)	PFC2D (kN)	Error (%)	Experimental (MPa)	PFC2D (MPa)	Error (%)						
68.5	71.7	4.7	29.82	30.3	1.7						

In this work, a block of jointed rock mass was simulated using a 2D SRM model. The calibrated BPM was used to develop a large-scale rock mass sample of 2 m × 1 m (width × height). The same particle size, used in the small-scale tests, was employed for the 2D SRM models. To study the effect of joint intensity on the impact-induced damage of rock masses, the block of the rock mass was assumed to have different joint intensities. The cumulated length of joint per total area of rock block (P_{21}) was considered to be representative of the joint intensity in the 2D simulation. In order to generate SRM samples with different joint intensities (P_{21}), three discrete joint networks with joint intensities (P_{21}) of 1 m^{-1}, 2 m^{-1} and 3 m^{-1} were incorporated into the large-scale BPM. The joint properties were simulated to be cohesionless with a friction angle of 30° and zero tensile strength. The bonds along the joint surface were deleted, and the stiffness and friction coefficient of balls along the joint surface were modified to normal stiffness of 10^{11} Pa, shear stiffness of 10^{10} Pa, and friction coefficient of 0.58 in order to achieve the mechanical properties of joints. Biaxial strength tests were simulated to assign the shear properties of the joint surface (Esmaieli et al., 2010). Joint size was considered to be fully persistent across the rock samples, and in this study, only the influence of joint spacing was investigated. The generated SRM samples for different joint intensities are shown in Fig. 6.

2.2.4. Impact-induced damage of jointed rock mass samples

Using the generated jointed rock mass samples, numerical impact tests were conducted to investigate the influence of joint intensity on the damage inflicted by particle impact. A 0.4 m diameter rock fragment with the density of 2700 kg/m^3 was generated and projected vertically against the SRM samples with an impact velocity of 15 m/s (Fig. 7). The impact velocity was selected so as to generate a strain rate in the dynamic regime (rate higher than 10^0 s^{-1}) (Field et al., 2004). In order to prevent surface wave reflection from the SRM sample sides, balls located in the right and left outer sides of the SRM samples were fixed in the x-direction.

The impact of projectile particle acting on a jointed rock mass creates a damage zone. The extent of damage depends on the size and shape of the projectile fragment, the impact velocity, and the rock mass properties. The impact of a rock fragment on a rock mass initially leads to the closure of pre-existing flaws. This is followed by elastic deformation of the rock mass in the area of impact, ejecting small rock particles from the rock mass surface, and creating a crater zone. Underneath the crater zone, a significant portion of the impact energy is utilized in crushing the rock material. Beyond the crushed zone, the rest of the impact energy can create cracks of various forms and lengths, including large radial and side cracks. Fig. 8 illustrates the impact-induced damage zones inflicted on a rock mass surface (Lindqvist et al., 1994). In this study, the initiation and growth of the impact-induced microcracks are considered to be a quantitative parameter for rock mass damage assessment. This is in agreement with the previous work by Kachanov (1986).

Fig. 9 illustrates the damage inflicted by the projectile rock fragment on rock mass samples of different joint intensities. For comparison purposes, the damage inflicted on the large-scale intact rock sample with no joints is also presented in Fig. 9a.

The results of numerical impact tests carried out on the generated SRM samples illustrate that shear and tension impact-induced microcracks were generated in the rock mass. The majority of the impact-induced microcracks are generated in tension. For all the rock mass models analyzed, the crushed zone is in the immediate vicinity of the impact point. The size of the crushed zone is almost the same for all rock mass samples. Around the crushed zone, a high-density microcrack zone, almost 0.2 m wide and deep, is generated. Beyond this region, median and radial cracks are initiated and propagated from this high-density microcrack zone.

Fig. 9 also illustrates the dependency of the microcrack patterns on rock mass joint intensity. As the rock mass joint intensity increases, the crack pattern and consequently the impact-induced damage inflicted to the rock mass become wider and deeper. Furthermore, as the joint intensity increases, the radial and side cracks propagate longer and deeper inside the rock mass samples. For the rock mass sample of low joint intensity, P_{21} = 1 m^{-1}, microcracks propagate from the crushed zone toward the joint surface and crack propagation stops when it reaches the pre-existing joint interface. For the two SRM samples, with higher joint intensities of P_{21} = 2 m^{-1} and 3 m^{-1}, microcracks initiate and propagate from the crushed zone downward the joint plane. It was also observed that some microcracks can initiate from the joint planes and propagate upward. These microcracks propagate almost perpendicular to the pre-existing joint surface. These results are in agreement with field observations on blast-induced damage in open pit mines which indicate that radial cracks can propagate into multiple rock blocks and they generally terminate against the pre-existing joints (Hagan, 1979; Hustrulid, 1999). Surveying of blast-induced damage in several open pit mines using LiDAR technology by Lupogo (2016) indicates that blast-induced fractures are created in preferred orientations, generally perpendicular to the dominant pre-existing discontinuities in the rock mass.

As the joint intensity (P_{21}) of SRM samples increases up to a certain level, more microcracks are initiated and propagate due to the impact loads. However, for the SRM samples with P_{21} of 2 m^{-1} and 3 m^{-1}, the developed numbers of microcracks are almost the same.

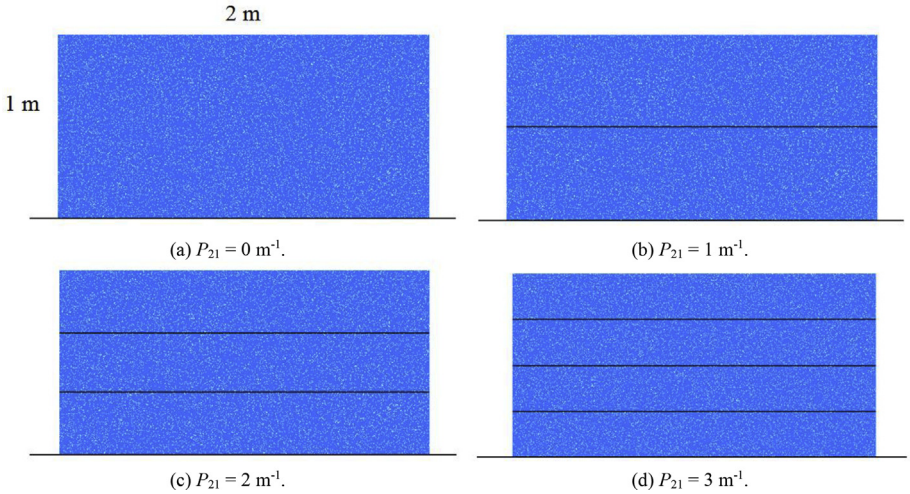

Fig. 6. Jointed rock mass samples with different joint intensities.

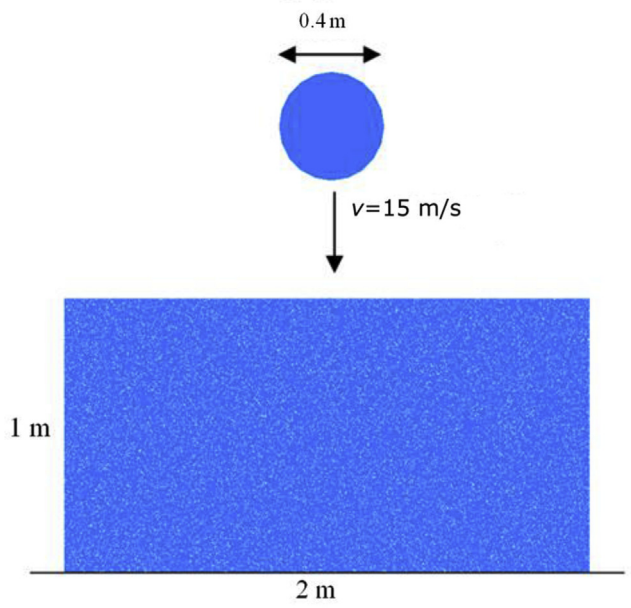

Fig. 7. Impact test on a jointed rock mass sample.

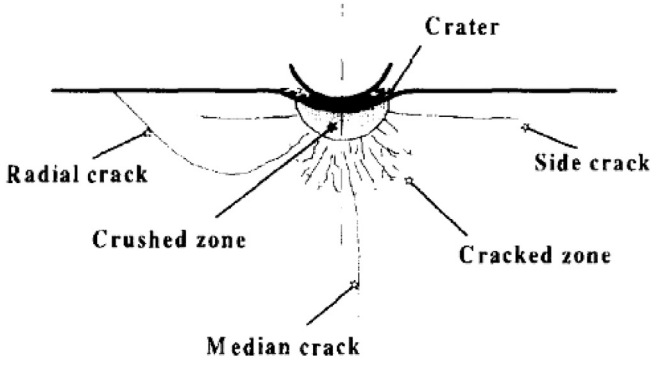

Fig. 8. General picture of crack system under impact in the longitudinal section (after Lindqvist et al., 1994).

Figs. 10 and 11 show the variation of particles velocity constituting the SRM samples with no joint ($P_{21} = 0$ m^{-1}) and with high joint intensity ($P_{21} = 3$ m^{-1}) during the impact test simulation. The results indicate that the presence of joints in the rock can significantly influence the propagation of stress waves in the rock samples. Part of the stress waves is reflected from the joint interface and this creates more cracks in the rock mass. The reflection of stress waves from the joint surface is attributed to the impedance mismatch between the rock material and the joint surface. As the joint intensity in the rock mass samples increases, more stress waves reflect from the joint interfaces as tensile wave. This will further fragment the rock matrix between the top free face of the sample and the joint interface, and between two consecutive joint surfaces. It shows that the experimental studies and numerical modeling on monoblock and multilayered plates by Zukas and Scheffler (2001) give similar forms of wave propagation.

It is interesting to note that the phenomenon observed in Figs. 10 and 11 has been also reported by Fourney (2015). Working with small-scale experimental blasting of a polymer material characterized with brittle behavior like rock, it was possible to demonstrate the reflection of shock waves from joint surfaces using dynamic photoelasticity. He observed that the presence of joints can drastically influence the propagation of blast-induced radial and median cracks. Additional fractures can originate from the joints surface that aids in rock fragmentation. These experimental results are consistent with the numerical experiments in the present work.

Fig. 12 illustrates the time histories of induced microcracks for the SRM samples with $P_{21} = 3$ m^{-1} and the sample with no joint ($P_{21} = 0$ m^{-1}). At the beginning of the impact process, the microcracks in the two rock samples are created with the same rate. The crack initiation rate for the sample with higher fracture intensity, $P_{21} = 3$ m^{-1}, was further increased after the time cycles of 7600. This occurred when the first impact-induced stress waves arrived to the upper joint surface in the jointed rock mass sample ($P_{21} = 3$ m^{-1}). Part of these waves were reflected from the joint surface interface and caused further damage to the rock mass. This was confirmed by monitoring the velocity of two particles (ball IDs 1 and 2 in Fig. 13) located in the opposite sides of the upper joint interface in the SRM sample with $P_{21} = 3$ m^{-1}. The same particles were also monitored for the sample without joints with $P_{21} = 0$ m^{-1}. The results are presented in Fig. 13, and it shows that the velocity of particles (ball IDs 1 and 2) for the sample with $P_{21} = 0$ m^{-1} (no joint) is almost identical. However, for the sample

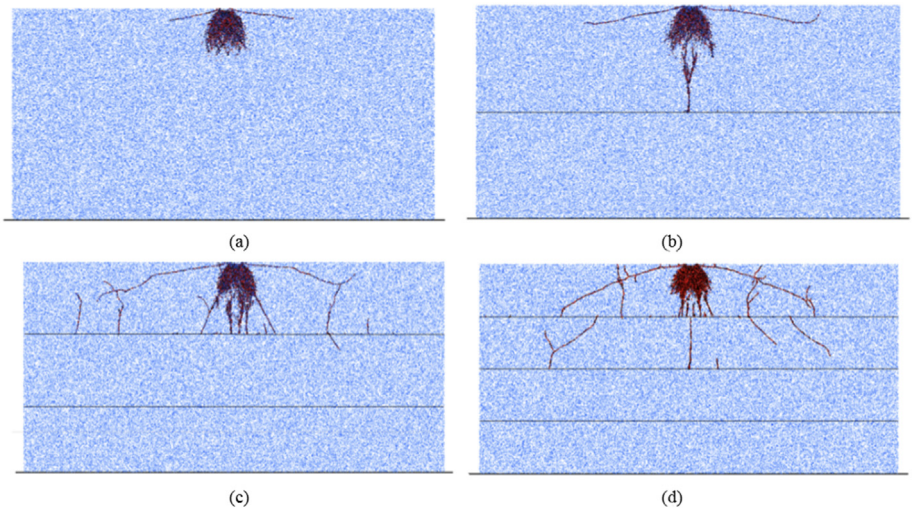

Fig. 9. Impact-induced damage within the rock mass samples with different joint intensities: (a) $P_{21} = 0\ m^{-1}$, (b) $P_{21} = 1\ m^{-1}$, (c) $P_{21} = 2\ m^{-1}$, and (d) $P_{21} = 3\ m^{-1}$. Tension and shear cracks are indicated in red and black, respectively.

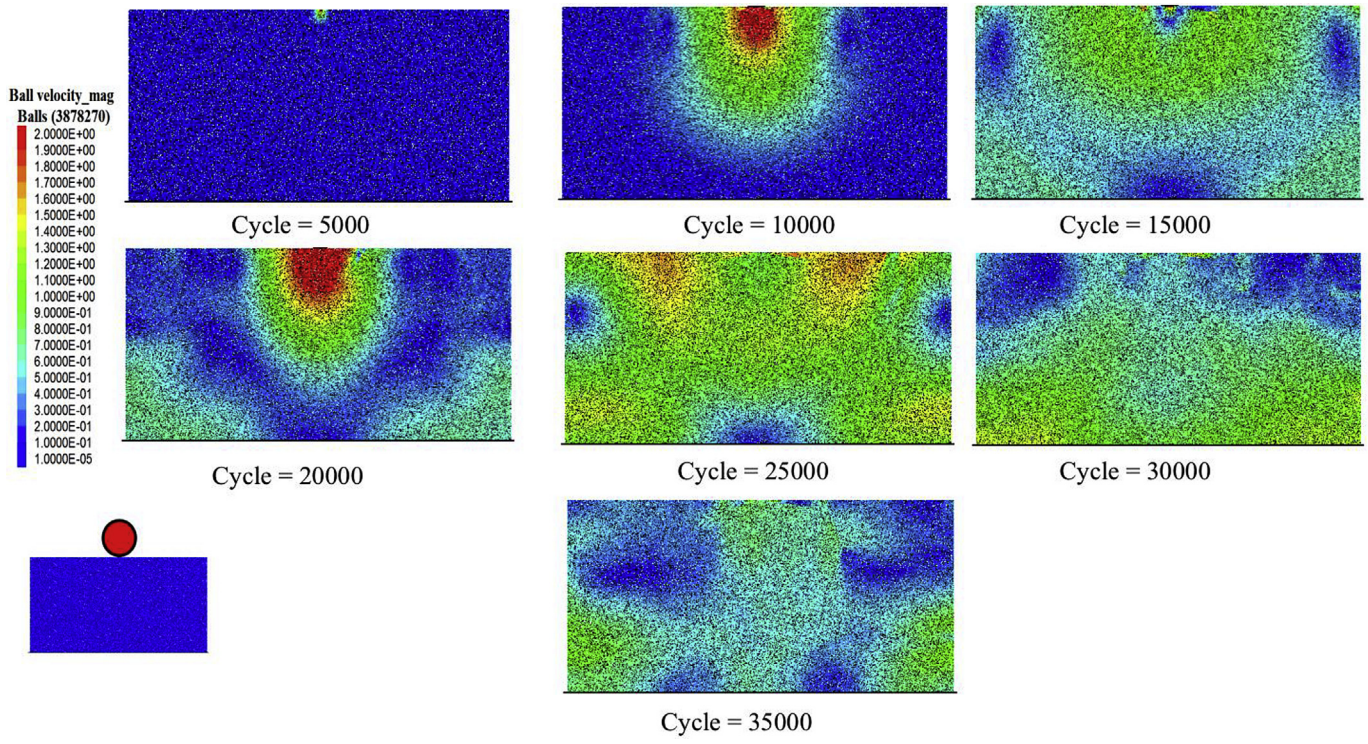

Fig. 10. Velocity contours of particles (m/s) constituting SRM sample with $P_{21} = 0\ m^{-1}$ at different stages of impact test simulation.

with $P_{21} = 3\ m^{-1}$, the amplitude of particle ball ID 1 (light blue color) is generally higher than the particle ball ID 2 (red line color). The considerable discrepancy between the two lines (red line and light blue line) indicates that multiple reflections and refractions of stress waves occurred in the joint plane. This figure also indicates that the stress waves in the jointed rock mass sample attenuate slower than the sample without any joints.

The large-scale impact tests presented in this study comprise of both loading and unloading phases. The loading phase starts when the projectile particle hits the jointed rock mass samples, and continues until the time cycles of 15,000. Subsequently, the projectile particle commences rebounding from the rock mass surface and triggers the unloading phase (after time cycles of 15,000). This unloading explains the increase in the particle velocity in the frames of time cycles of 20,000, and 25,000 (see Fig. 10) and the last three frames of time cycles of 25,000–30,000 (see Fig. 11). The unloading phase has been clearly identified in Fig. 13, where the direction of particle velocity (y-velocity) changes at about time cycles of 15,000, from negative to positive.

3. Conclusions

A number of laboratory tests were conducted to determine the static and dynamic properties of a meta-sandstone intact rock. This provided the experimental background to develop a series of numerical investigations. The BPM was successfully used to simulate

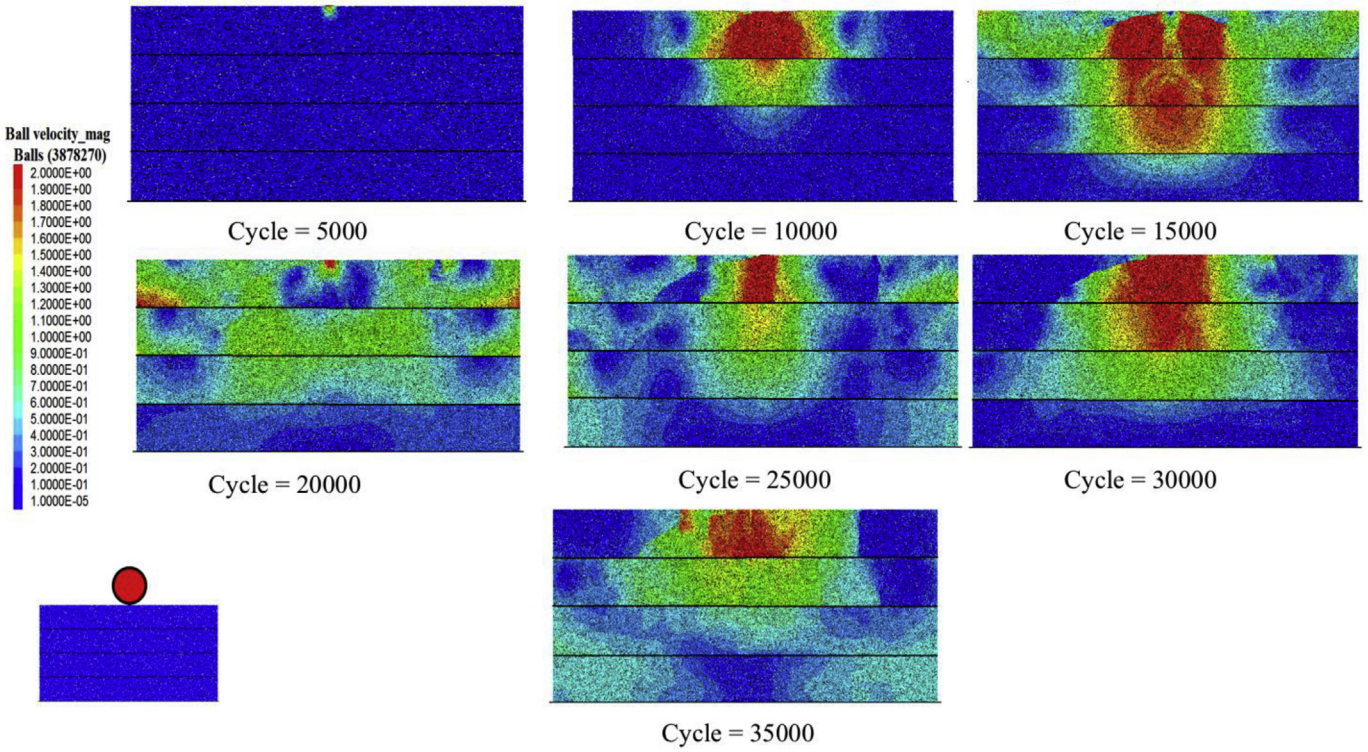

Fig. 11. Velocity contours of particles (m/s) constituting SRM sample with $P_{21} = 3\ m^{-1}$ at different stages of impact test simulation.

both the static and dynamic properties of the intact rock tested in the laboratory.

The BPM was calibrated against the experimental laboratory results. A major limitation of PFC models over the past decade was the inability to match the relatively large ratio of UCS to tensile strength of the intact rock. This was addressed in the present work by using the flat-joint contact model in intact rock calibration. Discrete joint networks of different intensities were incorporated into the calibrated BPM to simulate large-scale jointed rock mass samples. Finally, a rigid particle was projected against the jointed rock mass samples and the inflicted damage was quantified. In this study, damage was defined as the initiation and growth of micro-cracks within the numerical models.

The results of the impact simulation support the conclusion that the presence of structural defects within a rock mass plays a very important role in the impact-induced damage of the rock mass. Pre-existing joints influence the stress wave propagation in the rock mass samples and consequently the energy dissipation in the jointed rock mass samples. The impact-induced stress waves can reflect from joint surfaces and modify the crack pattern within the rock mass. Numerical results suggest that the radial cracks generally stop when they reach the pre-existing joints and are almost perpendicular to the joint surface. It is recognized that the higher intensity of joints within the rock mass results in more pronounced rock mass damage.

Since field or laboratory impact tests on large-scale rock mass samples are expensive and difficult to be carried out, numerical modeling provides a reasonably good understanding of the impact-induced damage mechanism and its complexity by the means of simplifications. The preference for 2D instead of 3D modeling in this paper was motivated by the shorter execution times for solving models. It is recognized that this simplified approach has some

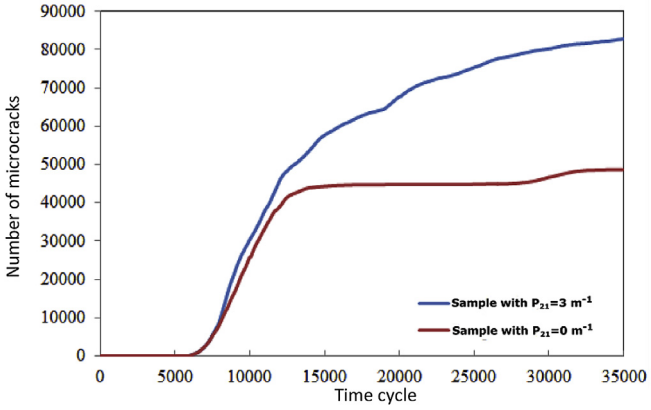

Fig. 12. Time histories of impact-induced microcracks for SRM samples with $P_{21} = 0\ m^{-1}$ and $P_{21} = 3\ m^{-1}$.

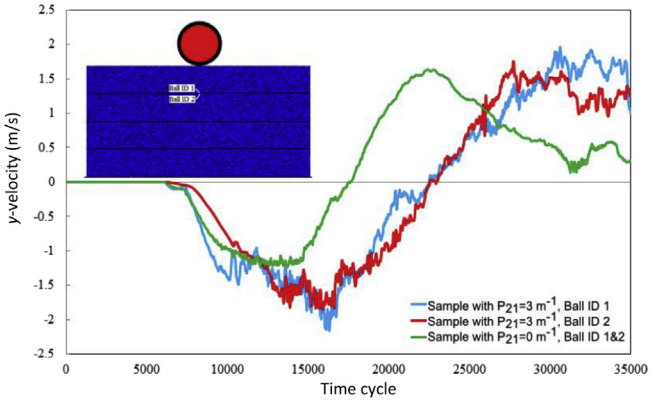

Fig. 13. Velocity histories of two particles on both sides of the defined joint for SRM sample with $P_{21} = 3\ m^{-1}$ and at the same location for the sample without joints.

inherent limitations. In general, 2D rock mass models can underestimate the rock mass mechanical properties. Nevertheless, the current work can eventually be extended to simulate this phenomenon in three dimensions.

Finally, this study helps to understand the impact-induced damage mechanism for jointed rock masses. The results of these investigations have significant implications in fragmentation and in material transfer during underground excavations in rock.

Conflict of interest

The authors wish to confirm that there are no known conflicts of interest associated with this publication and there has been no significant financial support for this work that could have influenced its outcome.

Acknowledgements

The authors would like to acknowledge the contribution of the CanmetMINING Rock Mechanics Laboratory, Natural Resources Canada, Ottawa, ON, Canada and the financial support provided by Natural Science and Engineering Research Council of Canada (NSERC) Grant No: RGPIN-2014-03992. The authors also appreciate access to the PFC code provided by Itasca through the IEP program.

References

Ahrens TJ, Rubin AM. Impact induced tensional failure in rock. Journal of Geophysical Research Planets 1993;98(1):1185–203.
ASTM D3967-08. Standard test method for splitting tensile strength of intact rock core specimens. West Conshohocken, PA, USA: ASTM International; 2008. p. 4.
ASTM D4543-08. Standard practices for preparing rock core as cylindrical test specimens and verifying conformance to dimensional and shape tolerances. West Conshohocken, PA, USA: ASTM International; 2008. p. 9.
ASTM D7012-14. Standard test method for compressive strength and elastic moduli of intact rock core specimens under varying states of stress and temperatures. West Conshohocken, PA, USA: ASTM International; 2014. p. 9.
Beus MJ, Iverson SR, Dreschler A, Scott VA. Static and dynamic loads in ore and waste rock passes in underground mines. In: Proceedings of the 37th U.S. Rock mechanics symposium. Vail, Colorado; 1999. p. 1–7.
Cadoni E. Mechanical characterization of rock materials at high strain-rate. In: Zhao J, Li J, editors. Rock dynamics and applications - state of the art. London: CRC Press; 2013. p. 137–47.
Camacho GT, Ortiz M. Computational modeling of impact damage in brittle materials. International Journal of Solids and Structures 1996;33(20–22):2899–938.
Cao P, Wang Y, Xia K. Testing study on damage fracture responses of rock under dynamic impact loading. Advanced Materials Research 2011;255–260:1815–9.
Cho N, Martin CD, Sego DC. A clumped particle model for rock. International Journal of Rock Mechanics and Mining Sciences 2007;44(7):997–1010.
Esmaieli K, Hadjigeorgiou J, Grenon M. Estimating geometrical and mechanical REV based on synthetic rock mass models at Brunswick Mine. International Journal of Rock Mechanics and Mining Sciences 2010;47(6):915–26.
Esmaieli K, Hadjigeorgiou J. Selecting ore pass-finger raise configurations in underground mines. Rock Mechanics and Rock Engineering 2011;44(3):291–303.
Esmaieli K, Hadjigeorgiou J. Impact-induced damage on foliated ore pass walls. CIM Journal 2014;5(1):39–47.
Esmaieli K, Hadjigeorgiou J, Grenon M. Capturing the complete stress-strain behavior of jointed rock using a numerical approach. International Journal for Numerical and Analytical Methods in Geomechanics 2015;39(10):1027–44.
Fakhimi A, Lanari M. DEM–SPH simulation of rock blasting. Computers and Geotechnics 2014;55(2):158–64.
Field JE, Walley SM, Proud WG, Goldrein HT, Siviour CR. Review of experimental techniques for high rate deformation and shock studies. International Journal of Impact Engineering 2004;30(7):725–75.
Fourney WL. The role of stress waves and fracture mechanics in fragmentation. In: Proceedings of the 11th international symposium on rock fragmentation by blasting, FragBlast11. Sydney, Australia; 2015. p. 27–39.
Gao F, Hou H, Yang X. Numerical analysis of dynamic mechanical properties for rock sample under strong impact loading. International Journal of Information Engineering and Electronic Business 2010;2(2):10–6.
Gong QM, Jiao YY, Zhao J. Numerical modelling of the effects of joint spacing on rock fragmentation by TBM cutters. Tunnelling and Underground Space Technology 2006;21(1):46–55.
Goodwill DJ, Craig DA, Cabrejos F. Ore pass design for reliable flow. Bulk Solid Handling 1999;19(1):13–21.
Grange S, Forquin P, Mencacci S, Hild F. On the dynamic fragmentation of two limestones using edge-on impact tests. International Journal of Impact Engineering 2008;35(9):977–91.
Hagan TN. Rock breakage by explosives. Acta Astronautica 1979;6(3–4):329–40.
Hiermaier S. Integrated experimental-numerical characterization of geological materials under shock and impact. In: Zhao J, Li J, editors. Rock dynamics and applications - state of the art. London: CRC Press; 2013. p. 71–6.
Hu L, Li Xi. Damage and fragmentation of rock under experiencing impact load. Journal of Central South University of Technology 2006;13(4):432–7.
Hustrulid W. Blasting principles for open pit mining, vol. 1. A.A. Balkema; 1999. p. 382.
Itasca. Particle flow code, PFC2D-V.5.0. Itasca Consulting Group, Inc.; 2016.
Kachanov LM. Introduction to continuum damage mechanics. Springer; 1986.
Lambert C, Coll C. Discrete modeling of rock joints with a smooth-joint contact model. Journal of Rock Mechanics and Geotechnical Engineering 2014;6(1):1–12.
Lindqvist PA, Suarez del Rio LM, Montoto M, Tan X, Kou S. Rock indentation database-testing procedures, results and main conclusions. 1994. SKB Project Report 44-94-023.
Lupogo K. Characterization of blast damage in rock slopes: an integrated field-numerical modelling approach. PhD Thesis. Canada: Simon Fraser University; 2016.
Mas Ivars D, Potyondy DO, Pierce M, Cundall PA. The smooth-joint contact model. In: Proceedings of the 8th world congress on computational mechanics/5th european congress on computational mechanics and applied science and engineering, June 30-July 4, 2008. Venice, Italy; 2008. Paper A2735.
Momber AW. Damage to rocks and cementitious materials from solid impact. Rock Mechanics and Rock Engineering 2003;37(1):57–82.
Nazeri H, Mustoe GGW, Rozgonyi TG, Wienecke CJ. Implementation of a discrete element methodology for the modeling of gravity flow of ore in ore passes. In: Hammah R, Bawden W, Curran J, Telesnicki M, editors. Proceedings of the 5th North American Rock Mechanics Symposium and 17th tunneling association of Canada. Toronto, Canada: University of Toronto Press; 2002. p. 1307–13.
Potyondy DO, Cundall PA. A bonded particle model for rock. International Journal of Rock Mechanics and Mining Sciences 2004;41(8):1329–64.
Potyondy DO. A grain-based model for rock: approaching the true microstructure. In: Proceedings of the rock mechanics in the Nordic Countries, Kongsberg, Norway, 9–12 June 2010. Norwegian Group for Rock Mechanics; 2010. p. 225–34.
Potyondy DO. A flat-jointed bonded-particle material for hard rock. In: Proceedings of the 46th U.S. Rock mechanics/geomechanics symposium. Chicago: 24–27 June 2012. American Rock Mechanics Association; 2012. ARMA-2012-501.
Potyondy DO. The bonded-particle model as a tool for rock mechanics research and application: current trends and future directions. Geosystem Engineering 2015;18(1):1–28.
Taylor LM, Chen EP, Kuszmaul JS. Microcracking-induced damage accumulation in brittle rock under dynamic loading. Computer Methods in Applied Mechanics and Engineering 1986;55(3):301–20.
Wang Y, Tonon F. Discrete element modeling of rock fragmentation upon impact in rock fall analysis. Rock Mechanics and Rock Engineering 2010;44(1):23–35.
Xia K, Ahrens TJ. Impact induced damage beneath craters. Geophysics Research Letter 2001;28(18):3525–7.
Yilmaz O, Unlu T. Three-dimensional numerical rock damage analysis under blasting load. Tunnelling and Underground Space Technology 2013;38:266–78.
Zukas JA, Scheffler DR. Impact effects in multilayered plates. International Journal of Solids and Structures 2001;38(19):3321–8.

Shabnam Aziznejad obtained her MSc degree in Mining Engineering from Lassonde Institute of Mining, University of Toronto, Canada. Since 2016 she is employed as a Geotechnical Engineer with Alston Associates, Toronto, Canada.

Dr. Kamran Esmaieli is an associate professor at Lassonde Institute of Mining, University of Toronto, Canada. Dr. Esmaieli has more than 15 years of international consulting and research experiences in mining engineering. His research topics include real-time acquisition of mining data, data integration, analytics and visualization, spatial models of rock mass geomechanical properties, numerical simulation of rock mass damage and the applications of synthetic rock mass modeling.

Prof. John Hadjigeorgiou holds the Pierre Lassonde Chair in Mining Engineering at the University of Toronto. Dr. Hadjigeorgiou is a P.Eng., with over 25 years of international consulting and research experience in mining engineering. John is a past recipient of the John Franklin Award from the Canadian Geotechnical Society and the Rock Mechanics Award from the Canadian Institute of Mining.

Denis Labrie obtained his bachelor and master degrees in mining engineering and rock mechanics from École Polytechnique de Montreal, Canada. He has more than 30 years of experience as lead rock mechanics research engineer with CanmetMINING laboratories, Natural Resources Canada.